Automatic Collision Avoidance for Teleoperated Underactuated Aerial Vehicles using Telemetric Measurements

Minh-Duc Hua, Tarek Hamel, Hala Rifai, Pascal Morin, Claude Samson

Automatic Collision Avoidance for Teleoperated Underactuated Aerial Vehicles using Telemetric Measurements

Minh-Duc Hua, Hala Rifai, Tarek Hamel, Pascal Morin, Claude Samson

Abstract

The paper deals with the obstacle avoidance problem for unmanned aerial vehicles (UAVs) operating in teleoperated mode. First, a feedback controller that we proposed recently for the stabilization of the UAV's linear velocity is recalled. Then, based on sensory measurements, a control strategy is proposed in order to modify the reference velocity on-line in the neighborhood of obstacles so as to avoid collisions. Both cases of telemetry and optical flow sensors are addressed. Stability properties of the proposed feedback controller are established based on a Lyapunov analysis. Simulations results are reported to illustrate the approach.

Keywords

Teleoperation; Collision avoidance; VTOL UAV; Telemetric measurement; Optical flow; Lyapunov stability.

I. Introduction

Unmanned aerial vehicles (UAVs) are mainly used for outdoor missions of surveillance and monitoring. In cluttered environments, obstacle avoidance is essential for the mission success and the vehicle's integrity. In this paper we are more specifically interested in teleoperated modes for small underactuated UAVs. Quite often, visual evaluation by the user of the distance between the UAV and surrounding obstacles is difficult. Therefore, an efficient automatic obstacle avoidance functionality is needed. This raises specific problems. First, the reference trajectory, which may be specified on-line by the user via a joystick, may not take obstacles into account. This advocates for a reactive approach to the obstacle avoidance problem, by opposition to a higher-level (planification-type) approach. Then, UAVs, especially small ones, are subjected to fast dynamics due to their size and limited actuation power. For example, they are highly sensitive to wind gusts. Obstacle avoidance solutions based on a purely kinematic analysis may fail, especially for the class of *underactuated* UAVs considered in this paper. This leads to take into account the system's dynamics in the obstacle avoidance strategy. In this paper, such a strategy is proposed together with a trajectory tracking controller, and the stability of the proposed solution is established. Interaction of the robot with surrounding obstacles is typically measured either by telemetric or optical flow sensors. We show that the proposed solution can be applied with both types of measurements.

Different strategies for obstacle avoidance have been developed in the context of UAVs. In [5], [24], vision based techniques are developed to detect obstacles, modify the UAV's trajectory by defining new waypoints, and manage the UAV's navigation between the waypoints via the minimization of some criterion. By contrast, the present paper addresses the teleoperation mode, for which the notion of waypoint does not apply. In [12], an

Minh-Duc Hua, Hala Rifai, and Tarek Hamel are with I3S UNSA–CRNS, Nice-Sophia Antipolis, France. E-mails: *minh.hua@polytechnique.org*, *rifai@i3s.unice.fr*, *thamel@i3s.unice.fr*.

Pacal Morin and Claude Samson are with INRIA, Sophia-Antipolis, France. E-mails: *Pascal.Morin@inria.fr*, *Claude.Samson@inria.fr*.

optimal control law is applied to ensure the obstacle avoidance based on a virtual space approach. The geometry of the obstacles is assumed to be known a priori and only the case of fixed-point stabilization is addressed. Obstacle avoidance is addressed in [1] for aircraft pursuit problems based on a geometric algorithm which minimizes the robot deviation from its nominal trajectory. The associated analysis relies on a kinematic motion model. In [23], a potential field approach combined with a state feedback is developed. Stability of the proposed solution is proved but only in the case of point mass dynamical models with the objective of fixed-point stabilization. The obstacle avoidance problem for planar guidance problems using radar measurements has been considered in [14], [22]. The vehicle's dynamics is not taken into account and the approach is dedicated essentially to airplanes or missiles rather than vertical take-off and landing vehicles (VTOLs). A biomimetic approach [2] based on optic flow sensors is presented in [20]. It consists in controlling the vehicle's velocity by regulating the optic flow relative to an obstacle in order to avoid collisions. The approach is developed in the planar case for a fully actuated vehicle. An optical flow based control approach for VTOLs is proposed in [6] for terrain-following. It consists in stabilizing a non-null constant horizontal velocity and a constant translational optical flow. Recently, the problem of obstacle avoidance for teleoperated UAVs has been considered in [16]. While the objectives are the same, the approach is different from the one presented here. Furthermore, only the case of optical flow measurements is addressed in [16] whereas we also consider telemetric measurements. In summary, even though the obstacle avoidance problem for UAVs has been addressed in the past, the specific case of teleoperation for underactuated vehicles has received little attention.

The strategy proposed in this paper can be used for a large family of VTOLs, including helicopters [13], [3], quadrotor helicopters [4], [21], and ducted-fan tailsitters [19]. These vehicles are underactuated in the sense that, apart from the direction associated with the thrust force, the other two directions of displacement are not directly actuated. Commonly, these vehicles move in 3D-space with four independent actuators (one thrust force and three torques), knowing that six actuators would be necessary for full actuation. First, a tracking controller proposed in [10] for this class of systems to asymptotically stabilize a reference translational velocity is recalled. Then, based on exteroceptive measurements, a strategy is proposed to modify this reference velocity when this is required to avoid obstacles. Stability properties of the proposed control scheme are established. Finally, simulation results are presented to illustrate the concept.

II. UAVs modeling and basics of control design

A. System modeling

Let us consider an underactuated UAV with a thrust force and full torque control. The following notation is used.

- $\mathcal{I}$ is an inertial frame, here chosen as the NED frame (North-East-Down). $\mathcal{B}$ is a body-fixed frame attached to the UAV with its origin coinciding with the UAV's center of mass G (see Fig. 1).
- The position of G expressed in $\mathcal{I}$ is denoted as $x \in \mathbb{R}^3$. The translational velocity of G expressed in $\mathcal{I}$ and $\mathcal{B}$ are denoted as $\dot{x} = (\dot{x}_1, \dot{x}_2, \dot{x}_3)^\top$ and $v = (v_1, v_2, v_3)^\top$. The UAV's orientation is represented by the rotation matrix $R \in \mathrm{SO}(3)$ from $\mathcal{B}$ to $\mathcal{I}$. The angular velocity of $\mathcal{B}$ w.r.t. $\mathcal{I}$, expressed in $\mathcal{B}$, is denoted as $\omega = (\omega_1, \omega_2, \omega_3)^\top$.
- The body's mass, and inertia matrix expressed in body frame are denoted as m and $\mathrm{I} \in \mathbb{R}^{3\times3}$.

• The thrust force control input and the vector of torque control inputs are denoted as $\mathrm{T} \in \mathbb{R}$ and $\Gamma \in \mathbb{R}^3$.

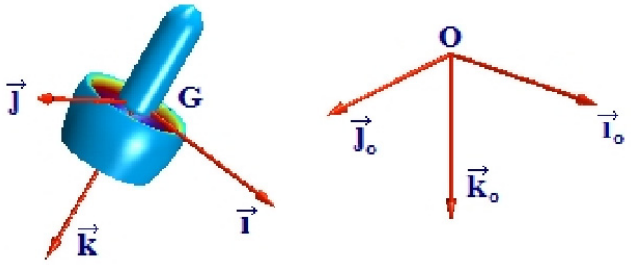

Fig. 1. Inertial and body-fixed frames.

By summing up all external forces acting on the vehicle (gravity, dissipative aerodynamic forces, etc.) in a vector $\overrightarrow{F}_e$, and by denoting the resulting torque induced by these external forces, expressed in $\mathcal{B}$, as Γ_e the equations of motion can be derived from the fundamental theorems of Mechanics (i.e. Euler-Newton formalism) (see e.g. [17], [10], [8])

$$\begin{aligned} \dot{x} &= Rv && (1)\\ m\dot{v} &= -m[\omega]_\times v - \mathrm{T}e_3 + R^\top F_e && (2)\\ \dot{R} &= R[\omega]_\times && (3)\\ \mathrm{I}\,\dot{\omega} &= -[\omega]_\times \mathrm{I}\,\omega + \Gamma + \Gamma_e && (4) \end{aligned}$$

with F_e the vector of coordinates expressed in $\mathcal{I}$ of $\overrightarrow{F}_e$, $e_3 := (0,0,1)^\top$, $[\omega]_\times$ the skew-symmetric matrix associated with the vector product (*i.e.* $[\omega]_\times a = \omega \times a$, $\forall a \in \mathbb{R}^3$). For later use, let us also define $e_1 := (1,0,0)^\top$ and $e_2 := (0,1,0)^\top$.

The knowledge of the external force F_e is very important for the control design. Several approaches can be used, depending on the available embarked sensors: direct measurement, estimation, or combination of both. Some solutions to this problem can be found in [8], [11]. In the present paper, for the sake of simplicity we assume that F_e is known with good accuracy.

From (4), the vehicle's orientation is fully actuated, and the exponential convergence of ω to any desired reference value can easily be achieved. As a consequence, ω can be seen as an intermediary vector control input of subsystem (1)–(3). This control strategy corresponds to the classical decoupled control architecture between inner and outer loops. In the sequel we focus on the control of the subsystem (1)–(3) using T and ω as the control inputs.

B. Basics of the control design

When obstacle avoidance is not considered, the basic control objective consists in stabilizing the UAV's velocity $\dot{x}$ to a reference value $\dot{x}_r \in \mathbb{R}^3$ which can be defined as a function of the joystick output $\dot{x}_\xi \in \mathbb{R}^3$. For instance, one can set

$$\dot{x}_r = \dot{x}_\xi. \qquad (5)$$

Define the velocity error $\dot{\widetilde{x}} := \dot{x} - \dot{x}_r$. Let $\widetilde{v} := v - R^\top \dot{x}_r$, so that $\widetilde{v} = R^\top \dot{\widetilde{x}}$. The control objective is equivalent to the stabilization of $\widetilde{v}$ to zero. A solution to this problem has been proposed in [10]. Let us recall this solution. Define

$$\gamma := F_e/m - \ddot{x}_r + h(|I_v|^2) I_v\,, \qquad (6)$$

$$\overline{\gamma} := \mathrm{R}^\top \gamma \,, \tag{7}$$

where $I_v(t) := \int_0^t (\dot{x}(s) - \dot{x}_r(s))\, ds + I_0$, with I_0 an arbitrary constant, and $h(\cdot)$ is some smooth bounded positive function defined on $[0, +\infty)$ and such that $|h(s^2)s| < \alpha\,,\ 0 < \frac{\partial}{\partial s}(h(s^2)s) < \beta\,, \forall s \in \mathbb{R}$, for some $\alpha,\ \beta > 0$. Let $\widetilde{\theta} \in (-\pi; \pi]$ denote the angle between the two vectors e_3 and $\overline{\gamma}$, so that $\cos\widetilde{\theta} = \overline{\gamma}_3/|\gamma|$, with $\overline{\gamma}_3$ the third component of $\overline{\gamma}$.

Proposition 1 *(See [10] for the proof) Apply the control law*

$$\begin{cases} \mathrm{T} \;=\; m(\overline{\gamma}_3 + |\gamma| k_1 \widetilde{v}_3) \\ \omega_1 = \; -|\gamma| k_2 \widetilde{v}_2 - \dfrac{k_3 |\gamma| \overline{\gamma}_2}{(|\gamma| + \overline{\gamma}_3)^2} - \dfrac{1}{|\gamma|^2} \gamma^\top S(Re_1) \dot{\gamma} \\ \omega_2 = \; |\gamma| k_2 \widetilde{v}_1 + \dfrac{k_3 |\gamma| \overline{\gamma}_1}{(|\gamma| + \overline{\gamma}_3)^2} - \dfrac{1}{|\gamma|^2} \gamma^\top S(Re_2) \dot{\gamma} \end{cases} \tag{8}$$

to system (1)–(3)*, with $k_{1,2,3}$ some positive constant gains and γ, $\overline{\gamma}$ defined by* (6), (7) *respectively. Assume that*

i) $\dot{x}_r$, $\ddot{x}_r$, $x_r^{(3)}$ are known and bounded;

ii) γ is always different from the null vector;

iii) ω_3 is bounded.

Then, for system (1)–(3) *complemented with the equation $\dot{I}_v = R\widetilde{v}$, the equilibrium point $(I_v, \widetilde{v}, \widetilde{\theta}) = (0, 0, 0)$ of the controlled system is asymptotically stable, with domain of attraction equal to $\mathbb{R}^3 \times \mathbb{R}^3 \times (-\pi, \pi)$.*

III. Collision avoidance using telemetric measurements

Let us consider a UAV moving close to an obstacle (e.g. a wall) which is detected by the embarked sensors. Assume that, locally, the obstacle's surface can be approximated by a plane so that one can define a vector $\overrightarrow{n}_0$ normal to the obstacle's surface and pointing away from the obstacle. We denote by n_0 the components of $\overrightarrow{n}_0$ expressed in $\mathcal{I}$ and assume that n_0 is known or can be extracted from the data provided by the embarked sensors, like e.g., *i)* a rotating radar or lidar fixed on a gyro-stabilized platform [18], *ii)* several laser range-finders or optical flow sensors pointing in different directions [7], or *iii)* a camera [15]. We also assume that the UAV is equipped with telemetric sensors allowing to measure the distance, denoted as d, between the UAV and the obstacle. Let

$$\eta := -\langle \dot{x}_\xi, n_0 \rangle \,, \tag{9}$$

with $\langle \cdot, \cdot \rangle$ the scalar product and $\dot{x}_\xi$ the reference velocity delivered by a joystick. A positive (resp. negative) value of η means that the UAV is commanded to move towards (resp. away from) the obstacle. The objective is to modify $\dot{x}_\xi$ so that the following objectives are met:

O.1) The UAV never collides with the obstacle;

O.2) If η is positive and constant, then the UAV asymptotically maintains a constant distance to the obstacle;

O.3) If η is negative and constant, then the UAV's velocity $\dot{x}$ converges to $\dot{x}_\xi$ so that the UAV ultimately moves away from the obstacle.

To this aim, instead of setting $\dot{x}_r$ equal to $\dot{x}_\xi$ one can set

$$\dot{x}_r = \dot{x}_\xi + \sigma n_0 \,, \tag{10}$$

where σ is a design term to be specified so that the three aforementioned objectives can be met. *Intuitively*, when $\dot{x}$ is stabilized to $\dot{x}_r$, i.e. $\dot{x} = \dot{x}_r$, one deduces from (10) that

$$\begin{array}{rcl} \dot{x} & = & \dot{x}_\xi + \sigma n_0 \\ \Rightarrow \quad \langle \dot{x}, n_0 \rangle & = & \langle \dot{x}_\xi, n_0 \rangle + \langle \sigma n_0, n_0 \rangle \\ \Leftrightarrow \quad \dot{d} & = & -\eta + \sigma, \end{array} \tag{11}$$

where $\dot{d}$, the time-derivative of d, satisfies $\dot{d} = \langle \dot{x}, n_0 \rangle$. The last equality in (11) suggests to choose σ as a static "potential" function $\chi(\cdot)$ of d (i.e. $\sigma \equiv \chi(d)$) which tends to infinity when d tends to zero and which vanishes when d is larger than a given threshold. Consider, for instance, a non-increasing smooth function $\chi(d)$ defined on $(0, +\infty)$ and satisfying the following three properties:

$$\frac{\partial \chi(d)}{\partial d} < 0, \forall d \in (0, d^*)\,, \tag{12}$$

$$\chi(d) = 0, \forall d \geq d^*\,, \tag{13}$$

$$\int_0^{d^*} \chi(s) ds = +\infty\,, \tag{14}$$

with d^* an arbitrary positive constant, then it is simple to verify that if $\sigma \equiv \chi(d)$ then the satisfaction of the last equality in (11) implies:

i) If $d(0) > 0$, then $d(t) > 0, \forall t$;
ii) If $\eta > 0$ and $\dot{\eta} = 0$, then d converges to d_e defined by $d_e := \chi^{-1}(\eta)$ with $\chi^{-1}(\cdot)$ the inverse function of $\chi(\cdot)$;
iii) If $\eta < 0$ and $\dot{\eta} = 0$, then $\dot{d}$ converges to $-\eta$.

More rigorously, without assuming that $\dot{x}(t) = \dot{x}_r(t), \forall t$, we state the following theorem (see Appendix A for the proof).

Theorem 1 *Apply the control law* (8) *to system* (1)–(3) *where the reference velocity* $\dot{x}_r$ *is defined by* (10) *and* σ *(involved in* $\dot{x}_r$*) is identical to a non-increasing smooth function* $\chi(\cdot)$ *of* d *(i.e.* $\sigma \equiv \chi(d)$*) satisfying Properties* (12)–(14)*. Assume that:*
H.1) d, $\dot{d}$, *and* $\ddot{d}$ *are known;*
H.2) $d(0)$ *is positive;*
H.3) $\dot{x}_\xi$, $\ddot{x}_\xi$, *and* $x_\xi^{(3)}$ *are known and bounded;*
H.4) Assumption ii) and iii) of Proposition 1 are satisfied.
Then, the results of Proposition 1 and the following properties hold:
1) There exists a constant $d_{min} > 0$ *such that* $d(t) \geq d_{min}, \forall t$.
2) If η *(defined by* (9)*) is positive and constant, then* d *converges to a positive constant* d_e *defined by* $d_e := \sigma^{-1}(\eta)$ *with* $\sigma^{-1}(\cdot)$ *the inverse function of* $\sigma(\cdot)$.
3) If η *is negative and constant, then* $\dot{x}$ *converges to* $\dot{x}_\xi$.

In view of (10), Assumption H.1 of Theorem 1 (i.e. the knowledge of d, $\dot{d}$, $\ddot{d}$) is necessary for the implementation of the control law (8) whose expression involves $\dot{x}_r$, $\ddot{x}_r$, and $x_r^{(3)}$ (the latter term is used in $\dot{\gamma}$). In practice, d can be obtained from telemetric measurement data with good accuracy. In turn, $\dot{d}$ (required to calculate $\ddot{x}_r$) and especially $\ddot{d}$ (required to calculate $x_r^{(3)}$) are more difficult to obtain. Several solutions can be used: estimation via a filter/estimator, calculation from the relations $\dot{d} = \langle \dot{x}, n_0 \rangle$, $\ddot{d} = \langle \ddot{x}, n_0 \rangle$ and the measurement/estimation of $\dot{x}$ and $\ddot{x}$. However, in any case, due to measurement noise

and errors, accurate estimation of high-order derivatives of d is difficult. In the following lemma (see Appendix B for the proof), we propose to modify σ so that Properties 1–3 of Theorem 1 can still be ensured without the requirement of knowing $\ddot{d}$ to implement the control law (8).

Lemma 1 *Apply the control law* (8) *to system* (1)–(3) *where the reference velocity* $\dot{x}_r$ *is defined by* (10) *and* σ *(involved in* $\dot{x}_r$*) is the solution to the following differential equation:*

$$\dot{\sigma} = -\kappa\sigma + \chi(d),\ \sigma(0) = 0\,, \tag{15}$$

where κ *is a positive gain and* $\chi(\cdot)$ *is a non-increasing smooth function defined on* $(0, +\infty)$ *and satisfying* (12)–(14)*, with an arbitrarily positive constant* d^**. Assume that:*
H.1) d *and* $\dot{d}$ *are known;*
H.2) $d(0)$ *is positive;*
H.3) $\dot{x}_\xi$*,* $\ddot{x}_\xi$*, and* $x_\xi^{(3)}$ *are known and bounded;*
H.4) Assumption ii) and iii) of Proposition 1 are satisfied.
Then, the results of Proposition 1 and Theorem 1 hold, where the constant d_e *involved in Property 2 of Theorem 1 is given by* $d_e := \chi^{-1}(\kappa\eta)$*, with* $\chi^{-1}(\cdot)$ *the inverse function of* $\chi(\cdot)$*.*

In view of Lemma 1, by defining σ as the solution to a first-order differential equation driven by d (i.e. System (15)), instead of a static function of d, one avoids using the second-order derivative of d. However, the knowledge of $\dot{d}$ is still required. Going further in this direction, if we also want to avoid using $\dot{d}$, a possible solution consists in defining σ as the solution to the following second-order differential equation driven by d:

$$\ddot{\sigma} + 2\xi\omega_0\dot{\sigma} + \omega_0^2\sigma - \chi(d) = 0,\ \sigma(0) = \dot{\sigma}(0) = 0\,,$$

with $\xi,\ \omega_0 > 0$, and $\chi(d)$ as specified in Lemma 1. Good performance in simulations supports this intuitive idea. However, a theoretical stability analysis is not available in this case.

IV. Adaptation to optical flow measurements

In this section we show how the result of the previous section (i.e. Lemma 1) can be adapted to situations where telemetric sensors are replaced by, or used in combination with, optical flow sensors. Assume that the UAV is equipped with one (or several) camera(s) and an IMU that provide the translational optical flow, denoted as ϕ (see e.g. [6]). When a planar textured obstacle is detected, the translational optical flow ϕ corresponds to $\dot{x}/d$, with $\dot{x}$ the UAV's velocity and d the distance between the UAV and the obstacle. Since the normal vector n_0 of the obstacle can be estimated (see e.g. [7] for a possible solution using several optical sensors pointing in different directions), the normal optical flow $\phi^\perp := -\langle\phi, n_0\rangle = -\dot{d}/d$ becomes available.

Lemma 2 *Apply the control law* (8) *to system* (1)–(3) *where the reference velocity* $\dot{x}_r$ *is defined by* (10) *and* σ *(involved in* $\dot{x}_r$*) is the solution to the following system:*

$$\left\{\begin{array}{lcl} \dot{\sigma} & = & -\kappa\sigma + \chi(e^\rho) \\ \dot{\rho} & = & -\phi^\perp \\ \sigma(0) & = & \rho(0) = 0 \end{array}\right. \tag{16}$$

where κ is a positive constant gain and $\chi(\cdot)$ is a non-increasing smooth function defined on $(0,+\infty)$ satisfying Properties (12)–(14) with $d^*=1$. Assume that:
H.1) $\phi^\perp$ is known;
H.2) $d(0)$ is positive;
H.3) $\dot{x}_\xi$, $\ddot{x}_\xi$, and $x_\xi^{(3)}$ are known and bounded;
H.4) Assumption ii) and iii) of Proposition 1 are satisfied.
Then, the results of Proposition 1 and Theorem 1 still hold, with d_e defined by $d_e := d(0)\chi^{-1}(\kappa\eta)$.

Proof: From the expression of $\dot{\rho}$ in (16) and $\phi^\perp = -\dot{d}/d$ one deduces that $\rho = \ln(d/d(0))$. As a consequence the expression of $\dot{\sigma}$ in (16) is equivalent to

$$\dot{\sigma} = -\kappa\sigma + \bar{\chi}(d)\,, \tag{17}$$

with $\bar{\chi}(d) := \chi(d/d(0))$. Since the function $\bar{\chi}(\cdot)$ also satisfies Properties (12)–(14) with $d^* = d(0)$ and (17) takes the same form as (15), Lemma 2 follows from Lemma 1. ∎

In fact, Lemma 2 is a direct result of Lemma 1. In this case, the information about d is obtained by means of integration of the normal optical flow $\phi^\perp$. In practice, this may be dangerous due to measurement noise and errors. Besides, it is worth noting that the optical flow is well detected only if the obstacle is textured enough. Another possibility of exploiting optical flow sensors consists in using them in combination with telemetric sensors. More precisely, one can obtain the distance to the obstacle d from telemetric sensors and deduce $\dot{d}$ from the normal optical flow $\phi^\perp$ and d according to $\dot{d} = -\phi^\perp d$. Then, the control strategy in Lemma 1 can be directly applied.

V. Simulation results

This section illustrates the proposed control approach for a model of a VTOL ducted-fan tail-sitter (see e.g. [18], [8] for more details on the system). The controller (8) is applied to subsystem (1)–(3), with the following gains and functions: $k_1 = 0.306$, $k_2 = 0.078$, $k_3 = 10$, $h(s) = \beta/\sqrt{1+\beta^2 s/\alpha^2}$, with $\alpha = 6$, $\beta = 2$. The desired yaw angular velocity is set to zero (i.e. $\omega_{d,3} = 0$). Then, a high gain controller is applied to subsystem (4) to stabilize the angular velocity at the desired value ω_d whose first two components are generated by the first controller (i.e. controller (8)). The applied control torque is computed according to $\Gamma = [\omega]_\times \mathrm{I}\omega_\mathrm{d} - \mathrm{I}K_\omega(\omega - \omega_\mathrm{d})$, with $K_\omega = \mathrm{diag}(20,20,20)$. The external force F_e and its time-derivative are not known exactly. They are estimated using a high gain observer, based on the measurement of the vehicle's velocity $\dot{x}$ and attitude R, as proposed in [9], [8].

Let us simulate the following scenario. There is no wind. The UAV's initial configuration is $x(0)=(-11,0,0)^\top, \dot{x}(0)=0$, $R(0) = I_3$. A vertical planar obstacle, with the normal vector $n_0 = -e_1$, is located at the origin of the inertial frame $\mathcal{I}$. The sensors, either telemetric or optical flow, are only able to detect the obstacle when the distance to the obstacle d is smaller than $d^* = 10\,(\mathrm{m})$. The second and third components of the reference velocity are set to zero whereas the first component of the reference velocity is given by

$$\dot{x}_{\xi,1}(t) = \begin{cases} 5\,, & \text{if} \quad 0(\mathrm{s}) < \mathrm{t} \leq 20(\mathrm{s}) \\ 10\,, & \text{if} \ \ 20(\mathrm{s}) < \mathrm{t} \leq 30(\mathrm{s}) \\ 10 + 3\sin(\pi t)\,, & \text{if} \ \ 30(\mathrm{s}) < \mathrm{t} \leq 40(\mathrm{s}) \\ 15\,, & \text{if} \ \ 40(\mathrm{s}) < \mathrm{t} \leq 60(\mathrm{s}) \\ 20\,, & \text{if} \ \ 60(\mathrm{s}) < \mathrm{t} \leq 80(\mathrm{s}) \\ -1\,, & \text{if} \qquad\quad t > 80(\mathrm{s}) \end{cases} \quad (\mathrm{m/s})$$

Two simulations are reported.

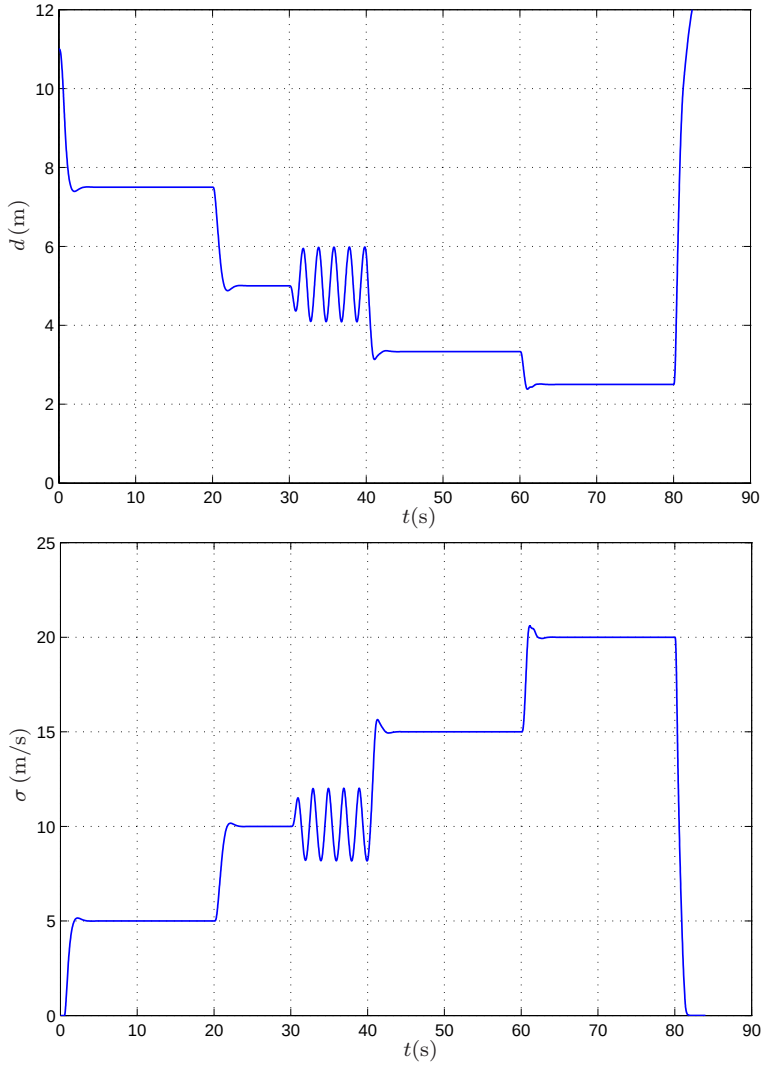

Fig. 2. d and σ vs. time – Simulation 1, with the use of d and $\dot{d}$.

▷ **Simulation 1 – with the use of d and $\dot{d}$ in the control law:** Assume that d is measured by telemetric sensors and $\dot{d}$ is estimated, either directly from d, or from the measurement of $\dot{x}$ and n_0, or by using the optical flow in combination with the measurement of d. The control strategy associated with collision avoidance proposed in Lemma 1 is applied. The dynamics of σ is given by (15), with $\kappa = 8$ and the function $\chi(\cdot)$ defined on $(0, +\infty)$ by

$$\chi(s) = \begin{cases} \kappa^* d^{*2}/(4s)\,, & \text{if } \; 0 < s \leq d^*/2 \\ \kappa^*(d^* - s)\,, & \text{if } \; d^*/2 < s \leq d^* \\ 0\,, & \text{if } \; s > d^* \end{cases} \tag{18}$$

with κ^*=16, d^*=10. Since d is measured, σ and $\dot{\sigma}$ are known from (15). As for $\ddot{\sigma}$, it can be computed as

$$\ddot{\sigma} = -\kappa\dot{\sigma} + \frac{\partial\chi(d)}{\partial d}\dot{d}\,.$$

Assuming that n_0 is constant and known, $\dot{x}_r$, $\ddot{x}_r$, and $x_r^{(3)}$ can be calculated according to (10), once σ, $\dot{\sigma}$, and $\ddot{\sigma}$ are available. The evolution of the distance d between the UAV

and the obstacle and the compensation term σ is shown on Fig. 2. The collision with the obstacle is avoided even when $\dot{x}_{\xi,1}$ is time-varying (e.g. $30\,(\mathrm{s}) \leq \mathrm{t} \leq 40\,(\mathrm{s})$) or very large (e.g. $60\,(\mathrm{s}) \leq \mathrm{t} \leq 80\,(\mathrm{s})$). Very fast convergence of d and σ can be observed when $\dot{x}_{\xi,1}$ is positive and constant. When $\dot{x}_{\xi,1}$ is negative (e.g. $t > 80\,(\mathrm{s})$), σ converges rapidly to zero.

▷ **Simulation 2 – without the use of $\dot{d}$ in the control law:** In order to test the robustness of the proposed control solution when $\dot{d}$ is not available, the incorrect value $\ddot{\sigma} = 0$ in the *case 1* where σ is calculated according to (15) with $\chi(d)$ used in Simulation 1, and incorrect values $\dot{\sigma} = 0$ and $\ddot{\sigma} = 0$ in the *case 2* where $\sigma \equiv \chi(d)$ are used in the control calculation. In the case 2 we have used the function (18) with κ^* equal to 2 (instead of 16) so that d_e is the same in both cases when $\dot{x}_{\xi,1}$ is a positive constant. The corresponding evolutions of d are shown on Fig. 3 and Fig. 4 respectively. In both cases, collision with the obstacle is avoided, although oscillations occur when $\dot{x}_{\xi,1}$ is large. Nevertheless, a better performance can be observed in the case 1.

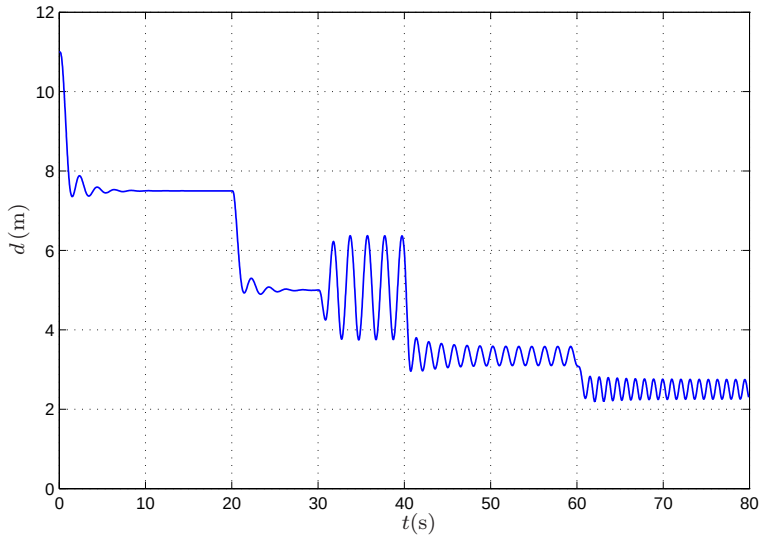

Fig. 3. d vs. time – Simulation 2, case 1 ($\dot{\sigma} = -\kappa\sigma + \chi(d)$, $\ddot{\sigma} = 0$).

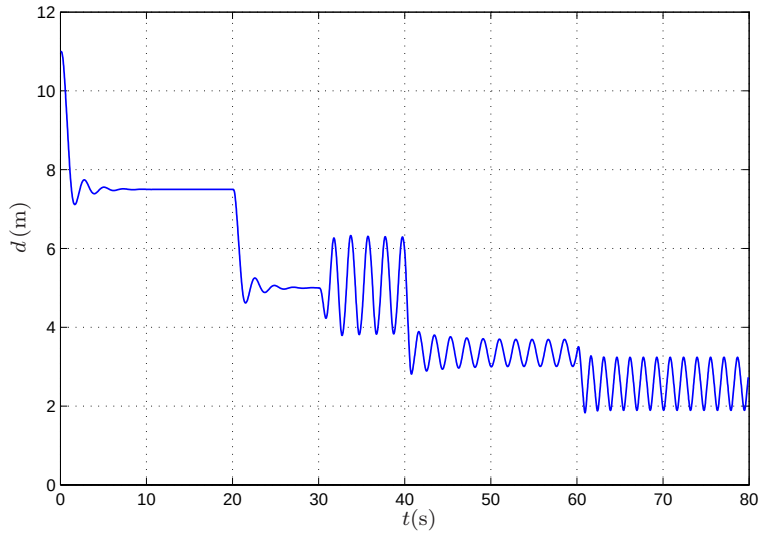

Fig. 4. d vs. time – Simulation 2, case 2 ($\sigma = \chi(d)$, $\dot{\sigma} = \ddot{\sigma} = 0$).

▷ **Simulation 3 – with optical flow measurements:** In this simulation, we assume that the translational optical flow $\phi^{\perp} = -\dot{d}/d$ can be extracted from the optical flow measurements. The control approach integrated with the collision avoidance strategy proposed in Lemma 2 is simulated, with $\kappa = 8$ and the function $\chi(\cdot)$ defined by (18) with $d^* = 1$ and $\kappa^* = 80$. The choice of the gain κ and the parameter κ^* involved in the function $\chi(\cdot)$ is justified by the fact that if initially $d_0 > 10(\text{m})$ (the value corresponding to d^* in Simulation 1), then the evolution of d is analogous to the one in Simulation 1. For instance, performing simulations with the same initial conditions and reference values as in Simulation 1, the evolutions of d and σ are exactly the same as the ones on Fig. 2.

As a result of Lemma 2, d_e (the value to which d converges when η is constant) is proportional to d_0 when $d_0 < 10(\text{m})$. Perform several simulations with different values of d_0 by changing the first component of the initial position. The evolution of d is described on Fig. 5. As expected, one can observe that when d_0 is large, very good performance is achieved even in the case of a large reference velocity $\dot{x}_{\xi,1}$ (i.e. η). In turn, when d_0 is small (i.e. the UAV starts from a point very close to the obstacle), poor damping occurs when the reference velocity $\dot{x}_{\xi,1}$ (i.e. η) is very large (e.g. $\dot{x}_{\xi,1} = 20(\text{m/s})$).

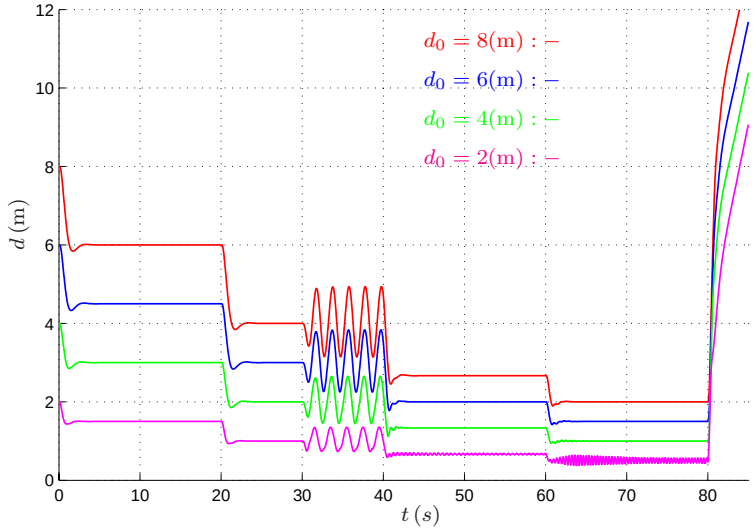

Fig. 5. d vs. time – Simulation 5, optical flow measurements

VI. Conclusion

A new control design approach has been proposed for the obstacle avoidance of teleoperated UAVs. It applies to both telemetric and optical flow measurements. It is based on an original on-line modification of the reference values set via the joystick. Simulation results have showed convincing performance. Among several possible perspectives the following ones can be proposed: 1) Gain tuning/scheduling in order to ensure a better damping close to the obstacle for high-intensity reference velocities; 2) Extension to haptic force feedback teleoperation; 3) Extension to wall following applications; and 4) Experimental validation.

References

[1] C. Carbone, U. Ciniglio, F. Corraro, and S. Luongo. A novel 3d geometric algorithm for aircraft autonomous collision avoidance. In *IEEE Conference on Decision and Control*, pages 1580–1585, 2006.

[2] N. Franceschini, J.-M. Pichon, C. Blames, and J.-M. Brady. From insect vision to robot vision [and discussion]. *Philosophical Transactions: Biological Sciences*, 337(1281):283–284, 1992.

[3] E. Frazzoli, M. A. Dahleh, and E. Feron. Trajectory tracking control design for autonomous helicopters using a backstepping algorithm. In *IEEE American Control Conference*, pages 4102–4107, 2000.
[4] T. Hamel, R. Mahony, R. Lozano, and J. Ostrowski. Dynamic modelling and configuration stabilization for an X4-flyer. In *IFAC World Congress*, pages 200–212, 2002.
[5] Z. He, R.-V. Iyer, and P.-R. Chandler. Vision-based UAV flight control and obstacle avoidance. In *IEEE American Control Conference*, pages 2166–2170, 2006.
[6] B. Hérissé, T. Hamel, R. Mahony, and F.-X. Russotto. A nonlinear terrain-following controller for a VTOL Unmanned Aerial Vehicle using translational optical flow. In *IEEE Conference on Robotics and Automation*, pages 3251–3257, 2009.
[7] B. Hérissé, S. Oustrières, T. Hamel, R. Mahony, and F-X. Russotto. A general optical flow based terrain-following strategy for a vtol uav using multiple views. In *IEEE Conference on Robotics and Automation*, pages 3341–3348, 2010.
[8] M.-D. Hua. *Contributions to the automatic control of aerial vehicles*. PhD thesis, Université de Nice-Sophia Antipolis, 2009. Available at http://tel.archives-ouvertes.fr/tel-00460801.
[9] M.-D Hua, T. Hamel, P. Morin, and C. Samson. Control of Thrust-Propelled Underactuated vehicles. Technical Report 6453, INRIA, 2008. Available at http://hal.inria.fr/inria-00258092/fr/.
[10] M.-D. Hua, T. Hamel, P. Morin, and C. Samson. A control approach for Thrust-Propelled Underactuated vehicles and its application to VTOL drones. *IEEE Transactions on Automatic Control*, 54(8):1837–1853, 2009.
[11] M.-D. Hua, P. Morin, and C. Samson. Balanced-Force-Control for Underactuated Thrust-Propelled vehicles. In *IEEE Conference on Decision and Control*, pages 6435–6441, 2007.
[12] T. Kobayashi, A. Ueda, J. Imae, and G. Zhai. Obstacle avoidance control of PVTOLs based on a virtual pace approach. In *IEEE International Conference on Networking, Sensing and Control*, pages 868–872, 2009.
[13] T. J. Koo and S. Sastry. Output tracking control design for a helicopter model based on approximate linearization. In *IEEE Conference on Decision and Control*, pages 3635–3640, 1998.
[14] B.A. Kumar and D. Ghose. Radar-assisted collision avoidance/guidance strategy for planar flight. *Transactions on Aerospace and Electronic Systems*, 37(1):77–90, 2001.
[15] Y. Ma, S. Soatto, J. Kosecka, and S. S. Sastry. *An Invitation to 3-D Vision: From Image to Geometric Models*. Springer Verlag, 2004.
[16] R. Mahony, F. Schill, P. Corke, and Y. S. Oh. A new framework for Force Feedback Teleoperation of Robotic vehicles based on Optical Flow. In *IEEE Conference on Robotics and Automation*, pages 1079–1085, 2009.
[17] R. M. Murray, Z. Li, and S. S. Sastry. *A mathematical introduction to robotic manipulation*. CRC Press, 1994.
[18] J.-M. Pflimlin. *Commande d'un minidrone à hélice carénée: de la stabilisation dans le vent à la navigation autonome (in French)*. PhD thesis, Ecole Doctorale Systèmes de Toulouse, 2006.
[19] J.-M. Pflimlin, P. Souères, and T. Hamel. Hovering flight stabilization in wind gusts for ducted fan UAV. In *IEEE Conference on Decision and Control*, pages 3491–3496, 2004.
[20] J. Serres, F. Ruffier, and N. Franceschini. Two optic flow regulators for speed control and obstacle avoidance. In *International Conference on Biomedical Robotics and Biomechatronics*, pages 750–757, 2006.
[21] A. Tayebi and S. McGilvray. Attitude stabilization of a VTOL quadrotor aircraft. *IEEE Transactions on Control Systems Technology*, 14(3):562–571, 2006.
[22] A. Viquerat, L. Blackhall, A. Reid, S. Sukkarieh, and G. Brooker. Reactive collision avoidance for unmanned aerial vehicles using doppler radar. In *6th International Conference on field and service robotics*, 2007.
[23] J. Wang, Xiaobei Wu, and Z. Xu. Potential-based obstacle avoidance in formation control. *Journal of Control Theory Applications*, 6(3):311–316, 2008.
[24] Y. Watanabe, A.-J. Calise, and E.-N. Johnson. Vision-based obstacle avoidance for UAVs. In *AIAA Guidance, Navigation and Control Conference and Exhibition*, 2007.

Appendix

I. Proof of Theorem 1

From (10) one verifies that

$$\langle \dot{\widetilde{x}}, n_0 \rangle = \langle \dot{x}, n_0 \rangle - \langle \dot{x}_r, n_0 \rangle = \dot{d} + \eta - \sigma. \tag{19}$$

Denoting $\psi := \eta - \langle \dot{\widetilde{x}}, n_0 \rangle$ one gets $\dot{d} = \sigma - \psi = \chi(d) - \psi$. First, one verifies that η is bounded. Besides, as a result of Proposition 1 $\dot{\widetilde{x}}$ is bounded. From here, one deduces that ψ is also bounded. One straightforwardly deduces from (12) and (14) that $\lim_{d\to 0^+} \chi(d) = +\infty$.

$\triangleright$ Let us prove Property 1. One verifies that the time-derivative of the function $\mathcal{S}_1 := 0.5(d-d^*)^2$ satisfies

$$\dot{\mathcal{S}}_1 \leq \chi(d)(d-d^*) + \sup(\psi)|d-d^*|\,,$$

with $\sup(\psi) = \max_{t\in(0,+\infty)} |\psi(t)|$. This inequality, the boundedness of ψ, and the fact that $\lim_{d\to 0^+} \chi(d) = +\infty$ ensure the existence of some positive constant d_- satisfying $d_- < d^*$ such that $\dot{\mathcal{S}}_1 < 0$ if $0 \leq d < d_-$. By denoting $d_{min} = \min(d_-, d(0))$, let us prove Property 1 by contradiction. Assume that there exists a time-instant $T > 0$ such that $d(T) < d_{min}$ and $d(t) \geq d_{min}, \forall t \in [0, T)$. This implies that $\dot{\mathcal{S}}_1(T) > 0$. But this contradict with the fact that $\dot{\mathcal{S}}_1(T) < 0$ since $d(T) < d_-$.

$\triangleright$ Let us prove Property 2. Since η is positive and constant, there exists a unique constant $d_e > 0$ satisfying $\chi(d_e) = \eta$. Then, one verifies that

$$\dot{d} = \chi(d) - \chi(d_e) + \varepsilon(\dot{\widetilde{x}}) \,,$$

with $\varepsilon(\dot{\widetilde{x}}) := \langle \dot{\widetilde{x}}, n_0 \rangle$ which is bounded and vanishes ultimately as a consequence of Proposition 1. The time-derivative of the candidate Lyapunov function $\mathcal{S}_2 := 0.5(d - d_e)^2$ satisfies

$$\dot{\mathcal{S}}_2 = (d - d_e)(\chi(d) - \chi(d_e)) + (d - d_e)\varepsilon(\dot{\widetilde{x}}) \,. \tag{20}$$

Let us prove that d is bounded. Since $\varepsilon(\dot{\widetilde{x}})$ converges to zero, there exists a time-instant τ such that $|\varepsilon(\dot{\widetilde{x}}(t))| \leq \chi(d_e)/2, \forall t \geq \tau$. This and (20) ensure the existence of some positive constant d_{max} such that $\forall t \geq \tau$, if $d(t) \geq d_{max}$ then $\dot{\mathcal{S}}_2(t) < 0$. Moreover, as proved previously in the proof of Property 1, σ, ψ and consequently $\dot{d}$ remain bounded which implies the uniform continuity of d. Consequently, d remains bounded in the limited period of time $[0, \tau]$. From here, it is straightforward to deduce that $\mathcal{S}_2$ remains bounded which in turn implies the boundedness of d. Then, one deduces from the boundedness of d the existence of a constant $\kappa_0 > 0$ such that

$$(d - d_e)(\chi(d) - \chi(d_e)) \leq -\kappa_0 (d - d_e)^2 \,.$$

From here, one deduces the existence of some other positive constants κ_1, κ_2 such that

$$\dot{\mathcal{S}}_2 \leq -\kappa_1 \mathcal{S}_2 + \kappa_2 \varepsilon(\dot{\widetilde{x}})^2 \,.$$

This inequality, the definition of $\mathcal{S}_2$, and the boundedness of $\varepsilon(\dot{\widetilde{x}})$ and its convergence to zero ensure the convergence of $\mathcal{S}_2$ to zero and consequently the convergence of d to d_e.

$\triangleright$ Let us prove Property 3. In this case η is a negative constant. One verifies that the candidate Lyapunov function $\mathcal{S}_3 := \int_d^{+\infty} \chi(s) ds$ satisfies

$$\dot{\mathcal{S}}_3 = -\chi(d)^2 + \chi(d)(\eta - \langle \dot{\widetilde{x}}, n_0 \rangle) \,.$$

Since $\dot{\widetilde{x}}$ converges to zero, there exists a time-instant T such that $\forall t \geq T, |\langle \dot{\widetilde{x}}, n_0 \rangle| \leq -\eta/2$. This and the fact that $\chi(d) \geq 0$ indicates that $\forall t \geq T$, $\dot{\mathcal{S}}_3(t) \leq 0$. One easily verifies that $\dot{\mathcal{S}}_3$ is uniformly continuous by verifying that $\ddot{\mathcal{S}}_3$ is bounded. Then, direct application of Barbalat's lemma ensures that $\dot{\mathcal{S}}_3$ converges to zero. This implies that $\chi(d)$ (i.e. σ) converges to zero. Since σ converges to zero, one deduces from (10) that $\dot{x}_r$ converges to $\dot{x}_\xi$. Since $\dot{\widetilde{x}}$ also converges to zero, the convergence of $\dot{x}$ to $\dot{x}_\xi$ is straightforward.

II. Proof of Lemma 1

Analogously to the proof of Theorem 1 one obtains $\dot{d} = \widetilde{\sigma} := \sigma - \psi$, with $\psi := \eta - \langle \dot{\widetilde{x}}, n_0 \rangle$. Then, using (15) one deduces

$$\dot{\widetilde{\sigma}} = -\kappa \widetilde{\sigma} + \chi(d) - (\kappa\psi + \dot{\psi}) \,. \tag{21}$$

As a result of the proof of Proposition 1 given in [10], $\dot{\widetilde{x}}$ and $\ddot{\widetilde{x}}$ are bounded. Besides, $\dot{x}_\xi$, $\ddot{x}_\xi$ are bounded by assumption. From here, one deduces that ψ, $\dot{\psi}$ are also bounded.
$\triangleright$ Let us prove Property 1. Consider the following Lyapunov-like function

$$\mathcal{S}_1 := 2\int_d^{d^*} \chi(s)ds + \widetilde{\sigma}^2 + \kappa\widetilde{\sigma}(d-d^*) + (\kappa^2/2)(d-d^*)^2\,. \tag{22}$$

From properties (14) and (12), one deduces that $\lim_{d\to 0^+}\chi(d) = +\infty$ and $\lim_{d\to 0^+}\mathcal{S}_1 = +\infty$. Using (21) and (22) one deduces that

$$\begin{aligned}\dot{\mathcal{S}}_1 &= -\kappa\widetilde{\sigma}^2 - 2(\kappa\psi+\dot{\psi})\widetilde{\sigma} + \kappa(\chi(d)-\kappa\psi-\dot{\psi})(d-d^*)\\ &\leq -\kappa\widetilde{\sigma}^2 + \kappa\chi(d)(d-d^*) + (2|\widetilde{\sigma}| + \kappa|d-d^*|)\sup(\kappa\psi+\dot{\psi}).\end{aligned}$$

This inequality implies that there exist some positive constants Δ_σ and d_- such that $\dot{\mathcal{S}}_1 < 0$, if $|\widetilde{\sigma}| > \Delta_\sigma$ or $0 < d < d_-$. This fact, together with the relation $\lim_{d\to 0^+}\mathcal{S}_1 = +\infty$ and $\mathcal{S}_1(0) < +\infty$, implies the existence of some other positive constants $\bar{\Delta}_\sigma \geq \Delta_\sigma$ and $d_{min} \leq d_-$ such that $|\widetilde{\sigma}| \leq \bar{\Delta}_\sigma$ and $d \geq d_{min}$.
$\triangleright$ Let us prove Property 2. Since η is a positive constant, there exists a unique positive constant d_e satisfying $\chi(d_e) = \kappa\eta$. Then, one verifies that (21) is equivalent to

$$\dot{\widetilde{\sigma}} = -\kappa\widetilde{\sigma} + \chi(d) - \chi(d_e) + \varepsilon(\dot{\widetilde{x}}, \ddot{\widetilde{x}})\,, \tag{23}$$

with $\varepsilon(\dot{\widetilde{x}}, \ddot{\widetilde{x}}) := \langle \kappa\dot{\widetilde{x}} + \ddot{\widetilde{x}}, n_0\rangle$ which is bounded and vanishes ultimately as a consequence of Proposition 1. Consider the following candidate Lyapunov function

$$\mathcal{S}_2 := 2\textstyle\int_d^{d_e}(\chi(s) - \chi(d_e))\,ds + \widetilde{\sigma}^2 + \kappa\widetilde{\sigma}(d-d_e) + (\kappa^2/2)(d-d_e)^2\,. \tag{24}$$

Since d is lower-bounded by a positive constant d_{min} (proved previously in the proof of Property 1), there exists a positive constant β_1 such that

$$\int_d^{d_e}(\chi(s) - \chi(d_e))\,ds \leq \beta_1(d-d_e)^2\,.$$

Thus, there exist some positive constants β_2, β_3 such that

$$\mathcal{S}_2 \leq \beta_2\widetilde{\sigma}^2 + \beta_3(d-d_e)^2\,. \tag{25}$$

From (23), (24), and the relation $\dot{d} = \widetilde{\sigma}$, one verifies that

$$\dot{\mathcal{S}}_2 = -\kappa\widetilde{\sigma}^2 + \kappa(d-d_e)(\chi(d)-\chi(d_e)) + \widetilde{\sigma}\varepsilon(\dot{\widetilde{x}}, \ddot{\widetilde{x}}) + \kappa(d-d_e)\varepsilon(\dot{\widetilde{x}}, \ddot{\widetilde{x}})\,. \tag{26}$$

Let us prove that d is bounded. As proved previously in the proof of Property 1, $\widetilde{\sigma}$ remains bounded. Since $\varepsilon(\dot{\widetilde{x}}, \ddot{\widetilde{x}})$ converges to zero, there exists a time instant τ such that

$$|\varepsilon(\dot{\widetilde{x}}(t), \ddot{\widetilde{x}}(t))| \leq \chi(d_e)/2,\ \forall t \geq \tau\,.$$

This, along with the boundedness of $\widetilde{\sigma}$ and relation (26), ensures the existence of a positive constant d_{max} such that $\forall t \geq \tau$, if $d(t) > d_{max}$ then $\dot{\mathcal{S}}_2(t) < 0$. Moreover, as a consequence of the uniform continuity of d (because $\dot{d}(=\widetilde{\sigma})$ is bounded), d is bounded in the limited period of time $[0, \tau]$. Then, these properties, along with the boundedness of $\widetilde{\sigma}$ and relation

(25), imply that d remains bounded. In turn, one deduces from the boundedness of d the existence of a constant $\beta_4 > 0$ such that

$$\kappa(d - d_e)(\chi(d) - \chi(d_e)) \leq -\beta_4 (d - d_e)^2 \,.$$

Then, one verifies from this inequality, (26) and (25) that there exist some positive constants α_1, α_2, α_3, λ such that

$$\begin{array}{rl} \dot{\mathcal{S}}_2 \leq & -\alpha_1 \widetilde{\sigma}^2 - \alpha_2 (d - d_e)^2 + \lambda \varepsilon(\dot{\widetilde{x}}, \ddot{\widetilde{x}})^2 \\ \leq & -\alpha_3 \mathcal{S}_2 + \lambda \varepsilon(\dot{\widetilde{x}}, \ddot{\widetilde{x}})^2. \end{array}$$

From this inequality and the convergence of $\varepsilon(\dot{\widetilde{x}}, \ddot{\widetilde{x}})$ to zero, one ensures that $\mathcal{S}_2$ asymptotically converges to zero. This, in turn, implies the convergence of $\widetilde{\sigma}$ to zero and of d to d_e.

$\triangleright$ Let us prove Property 3. In this case η is a negative constant. One verifies that the time-derivative of the candidate Lyapunov function

$$\mathcal{S}_3 := \int_d^{+\infty} \chi(s) ds + 0.5 \sigma^2$$

satisfies

$$\dot{\mathcal{S}}_3 = -\kappa \sigma^2 + \chi(d)(\eta - \langle \dot{\widetilde{x}}, n_0 \rangle) \,.$$

From here, one can proceed similarly to the proof of Property 3 of Theorem 1 to deduce the convergence of $\dot{\mathcal{S}}_3$, and subsequently of σ, to zero. Then, one easily deduces the convergence of $\dot{x}$ to $\dot{x}_\xi$.